Topical Review

A comprehensive survey on 'circular polarized antennas' for existing and emerging wireless communication technologies

Iram Nadeem[1] , **Mohammad Alibakhshikenari[2],*** , **Fatemeh Babaeian[3],**
Ayman A Althuwayb[4] , **Bal S Virdee[5], Leyre Azpilicueta[6], Salahuddin Khan[7],**
Isabelle Huynen[8] , **Francisco Falcone[9,10], Tayeb A Denidni[11] and Ernesto Limiti[12]**

[1] Information Engineering and Mathematics Department, University of Siena, 53100 Siena, Italy
[2] Department of Signal Theory and Communications, Universidad Carlos III de Madrid, 28911 Leganés, Madrid, Spain
[3] Department of Electrical and Computer Systems Engineering, Monash University, Melbourne, Australia
[4] Electrical Engineering Department, Jouf University, Sakaka, Aljouf 72388, Saudi Arabia
[5] Center for Communications Technology, London Metropolitan University, N7 8DB London, United Kingdom
[6] School of Engineering and Sciences, Tecnologico de Monterrey, Monterrey 64849, Mexico
[7] College of Engineering, King Saud University, Riyadh, Saudi Arabia
[8] Institute of Information and Communication Technologies, Electronics and Applied Mathematics, Université Catholique de Louvain, 1348 Louvain-la-Neuve, Belgium
[9] Electric, Electronic and Communication Engineering Department, Public University of Navarre, 31006 Pamplona, Spain
[10] Institute of Smart Cities, Public University of Navarre, 31006 Pamplona, Spain
[11] Institut National de la Recherche Scientifique (INRS), Université du Quebec, Montreal, QC, Canada
[12] Electronic Engineering Department, University of Rome 'Tor Vergata', Via Del Politecnico 1, 00133 Rome, Italy

E-mail: mohammad.alibakhshikenari@uc3m.es

CrossMark

Abstract

Circular polarized (CP) antennas are well suited for long-distance transmission attainment. In order to be adaptable for beyond 5G communication, a detailed and systematic investigation of their important conventional features is required for expected enhancements. The existing designs employing millimeter wave, microwave, and ultra-wideband (UWB) frequencies form the elementary platform for future studies. The 3.4–3.8 GHz frequency band has been identified

* Author to whom any correspondence should be addressed.

as a worthy candidate for 5G communications because of spectrum availability. This band comes under UWB frequencies (3.1–10.6 GHz). In this survey, a review of CP antennas in the selected areas to improve the understanding of early-stage researchers specially experienced antenna designers has presented for the first time as best of our knowledge. Design implementations involving size, axial ratio, efficiency, and gain improvements are covered in detail. Besides that, various design approaches to realize CP antennas including (a) printed CP antennas based on parasitic or slotted elements, (b) dielectric resonator CP antennas, (c) reconfigurable CP antennas, (d) substrate integrated waveguide CP antennas, (e) fractal CP antennas, (f) hybrid techniques CP antennas, and (g) 3D printing CP antennas with single and multiple feeding structures have investigated and analyzed. The aim of this work is to provide necessary guidance for the selection of CP antenna geometries in terms of the required dimensions, available bandwidth, gain, and useful materials for the integration and realization in future communication systems.

(Some figures may appear in color only in the online journal)

1. Introduction

Today, with the rapid development of wireless communication coupled with the handheld mobile and other portable devices, demand for a circular polarized (CP) antenna with wide impedance and axial-ratio (AR) bandwidth has been increased [1]. The ultra-wideband (UWB) CP antennas are widely used in military aspects such as electronic countermeasure systems, medical applications, and UWB radar systems [2, 3]. Moreover, modern communication systems such as mobile, navigation, and satellite applications are getting performance improvement by taking advantage of CP radiation pattern [4, 5]. CP antennas are becoming popular as they can receive all orientations of signals [6], reduce the multipath losses in the environment, and be sustainable to inclement weather [7, 8]. Interest in the CP characteristics of microstrip antennas grew predominantly due to its aptitude to support higher data rates and allowing flexibility of receiver orientation [9]. CP minimizes the sensitivity of orientations between the receiving and transmitting antennas. It can ease multipath interference in contrast to linear polarized (LP) [10, 11]. The attractive benefit of CP antennas is that it can send and receive signals in all planes having strong absorption and reflection of radio signals [12]. Also, CP overcomes phase problems in a multipath fading channel environment. This includes deadspots, decreased throughput, and reduced overall performance [13]. Additionally, compared to other polarizations, CP is more resistant to signal degradation due to extreme weather conditions [14, 15]. Although in the literature, many articles on high gain mmWave antenna arrays focus on the LP radiation, antennas with polarization diversity (circular or elliptical) can increase channel capacity [16, 17]. Hence, a study on CP antennas is beneficial for future developments in 5G and beyond wireless communications. The global rollout and growing popularity of 5G communications systems demonstrates that mmWave frequencies can be efficiently used for commercial wireless communications systems. Moreover, the Federal Communications Commission has granted the 95 GHz to 3 THz frequency band for 6G research. Until a few years ago mmWave was considered unrealistic because of the unfavorable propagation characteristics of these frequencies. Even though the 5G systems are still being rolled out, it is argued that the gigabit-per-second rates to be supported by the 5G mmWave systems may fall short in supporting many emerging applications, such as 3D gaming and extended reality. Such applications will require several hundreds of gigabits per second to several terabits per second data rates with high reliability and low latency. These are currently considered to be the design goals for the next generation 6G communications systems. It gives the potential of THz communications systems to provide such rates over short distances.

In this review paper, a comparative study on different methods to realize CP antennas with single and multiple ports has presented for the first time as best of our knowledge. Furthermore, various 3D antennas based on standard mutual coupling techniques have investigated to clarify design variation possibilities. Multiple input multiple output (MIMO) antennas presented in this work have discussed and compared with an emphasis on the primary antenna characteristics such as AR bandwidth and gain. This work highlights the usefulness and limitations of different CP antenna topologies existing in the literature. Furthermore, it also offers a thorough analysis of different CP antenna topologies to improve the understanding of early-stage researchers as well as experienced antenna designers.

This survey is organized as follows: section 2 briefly explains the three types of polarizations systems for emerging wireless communication networks. Section 3 provides a comprehensive study on the design challenges to achieve CP specifications in single and MIMO antenna technologies, with specific application examples for the different CP antennas. State-of-the-art comparison section has been presented in section 4. Finally, section 5 provides conclusion remarks.
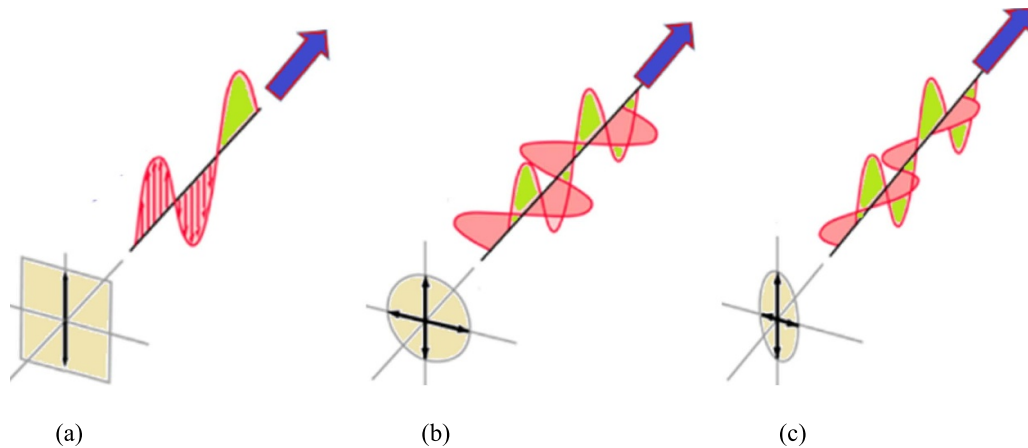
Figure 1. Three types of polarizations, (a) LP, (b) CP, and (c) EP.

2. Definition of the three types of polarizations; LP, CP, and EP

Polarization is the electromagnetic wave property that describes the time-varying direction and relative magnitude of the electric field vector along the direction of propagation. On the basis of AR, polarization is divided into three types known as LP, CP, and elliptical polarization (EP) as shown in figure 1 [4, 18–23].

LP of an electromagnetic wave consists of an electric vector at some point in space pointing in a fixed direction but can be in varying magnitude. It has two forms (a) horizontal, where the electric field is parallel to the earth's surface, and (b) vertical, where the electric field is perpendicular to the earth's surface, as shown in figure 1(a). However, both directions can be used simultaneously at the same frequency. In communication, transmitting and receiving antennas should be similarly polarized; otherwise, high loss in the system will occur. In the case of LP, the transmitting and receiving antennas are required to be appropriately aligned.

In CP the radiation is a superposition between two orthogonal LPs. CP can remove the limitation of alignment between the transmitter and receiver antennas [18, 19]. Because in this case, the electromagnetic field of the wave has a constant magnitude, and its direction rotates at a constant rate in a plane perpendicular to the direction of the wave, as exhibited in figure 1(b). Similarly, the radiation of an EP, shown in figure 1(c), is a superposition between two orthogonal LPs however of different magnitudes. CP can be achieved by two orthogonal components of the E-field vector in the exact phase quadrature [19]. The logic of CP is determined by the direction of the E-field vector rotation as it defines a circle. The polarization plane rotates in a specific pattern by creating one complete revolution during every wavelength. So, clockwise rotation looking in the propagation direction is known as right hand circular polarization (RHCP) [20]. Similarly, if the polarization rotation is anti/counter clockwise in the direction of propagation, then it is known as left-hand-circular-polarized (LHCP) [20]. A performance parameter comparison between circularly and non-circularly polarized antenna

in terms of radiation pattern can be made. A non-circularly polarized antenna (linear-polarized antenna) concentrates RF energy in a narrow plane, while circular-polarized antenna works to emit energy in a cockscrew fashion as it travels away from the antenna in free-space. The corkscrew becomes larger as the energy propagates further away from the antenna. Moreover, in case of LP, the magnitude of the received power at the antenna can be small as the diversity gain is limited.

3. Techniques for CP antenna designs

This section provides an overview of the design of CP antennas by using different feeding mechanisms of single and multiple feeds. In the literature, there are various approaches to produce CP antennas such as (a) printed CP antennas, (b) dielectric resonator CP antennas, (c) reconfigurable CP antennas, (d) substrate integrated waveguide (SIW) CP antennas, (e) fractal CP antennas, (f) hybrid techniques CP antennas, (g) 3D printing CP antennas, and (h) coplanar waveguide (CPW) feed CP antennas, which have been studied in below.

3.1. Printed CP antennas

A printed CP antenna is popular in the design of wireless communications owing to its lightweight, low profile, and ease to mass production. This technique has been used in both single port antennas and multiple antennas. There are a variety of approaches in the literature for printed CP antennas. In this section, a few examples have reviewed and discussed.

One approach to produce CP antennas in a printed structure is to utilize parasitic or slotted elements. Parasitic or slot element is a conductive plate, rod or cut-outs [24]. The size and shape of the slot and the driving frequency determine the radiation pattern of the antenna [25, 26]. Its main advantages are the simplicity of design and its suitable adaptation to mass production using either printed circuit (PC) board technology or waveguide [27, 28]. Microstrip CP antennas with a variety of designs are widely used in the literature [29–33].
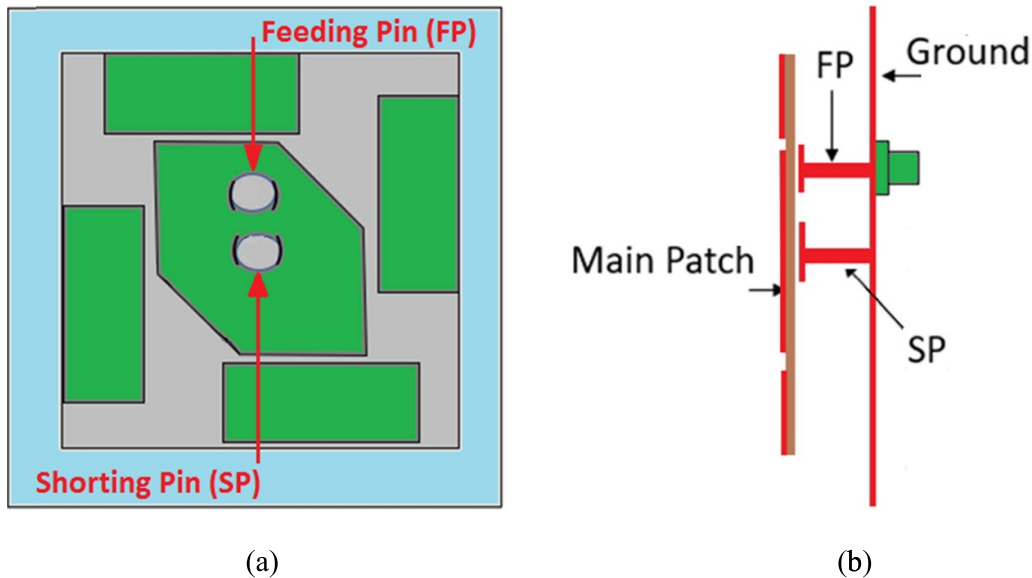
Figure 2. Printed CP patch antenna based on the parasitic elements, (a) top-view, and (b) side-view. © 2015 IEEE. Reprinted, with permission, from [31].

As an example of this type of antenna, figure 2 illustrates the original corner-truncated patch, sequential rotated four parasitic strips, and gap-coupled around the patch [29–31]. For wideband impedance-matching a capacitive coupled feed has utilized. Moreover, a disc-loaded shorting pin is below the center of the main patch for radiation pattern tuning and improves the gain along $+Z$ direction. The capacitance between the disc and patch can compensate the feed probe inductances, and consequently good impedance matching is achieved.

This antenna produces 9.3 dBi gain in an array of 5×5, and a 3 dB AR bandwidth of 8.1%. Similarly, another CP antenna consists of a circular patch with a central feed coaxial probe feed, eight open slots, and eight shorted metal pins has reported in [34]. The other example of printed CP with a single feed using a capacitive feeding and an upper parasitic notched patch introduced in [35] produces a conical beam. This antenna yields a 3 dB AR bandwidth of 10%.

In addition to single element antennas, printed CP antennas are developed for MIMO feed CP antennas. As an example, two orthogonal feed probes for CP excitation is employed with slot antenna given in [36]. Figure 3 shows a slot structure with an integrated compact UWB phase shifter and demonstrates an optimization technique using spline curves. The design consists of three metallization layers, separated by a substrate of a very minimum width of 0.5 mm. A UWB phase is incorporated into the antenna for the phase shift of 90°. It has two microstrip lines, running parallel on opposite sides of the ground-plane. An elliptical patch is loaded with each microstrip line, and both patches are coupled through a slot in the ground-plane. The location of the ports on the different layers simplifies the structure without any via connections. However, it provides a separation of 1 mm along the z-direction which cannot be reduced. The reason behind is that its thickness is articulated by phase shifter coupling properties. The ground-plane single closed spline loop is formed by the
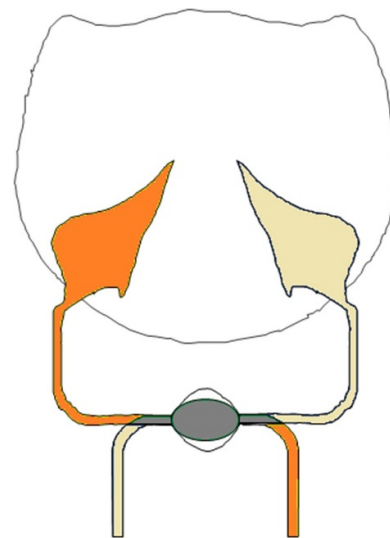

Figure 3. Geometry of UWB dual-feed CP antenna with spline curves. © 2015 IEEE. Reprinted, with permission, from [36].

angle of optimization α. Meanwhile, one spline control point moves in single dimension around the angle α. The slots allow confinement of the electric field and produces a bidirectional pattern.

The probes at the lower side of the substrate establish two orthogonal electric field components. This antenna has achieved a circularly polarized bandwidth of 54% covering an operating frequency range of 3.2–6.1 GHz (5G) with a gain of 1.6 dBi.

Further examples of compact CP MIMO planar antennas have reported in [37–39]. A dipole-like structure with 77% AR bandwidth, a hexagonal slot antenna with 50% AR bandwidth, and an L-shaped slot antenna providing 46.5% AR bandwidth for more complex geometries have been presented in [37–39], respectively.
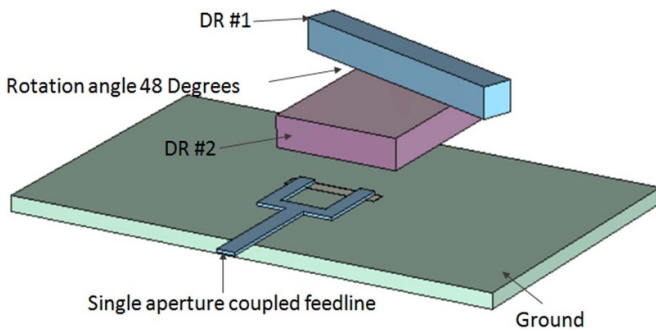
J. Phys. D: Appl. Phys. **55** (2022) 033002

Topical Review

Figure 4. Rectangular DRA with single aperture feed line. © 2015 IEEE. Reprinted, with permission, from [44].

Figure 5. Geometry of DRA with Archimedean slot excitation. © 2015 IEEE. Reprinted, with permission, from [45].

Figure 6. Dual feed decoupling network antenna. © 2015 IEEE. Reprinted, with permission, from [46].

3.2. Dielectric resonator CP antennas

Dielectric resonator antennas (DRA) [40] have received a lot of attention in the last two decades due to their attractive characteristics such as moderate bandwidth, low-temperature coefficient, and high radiation efficiency [41–43].

In [44], wideband CP DRA employing rotated-stair dielectric resonator is presented, as shown in figure 4. This design has a single aperture-coupled feed and two rectangular dielectric layers (dielectric resonators 1 and 2), having rotation angle ¥ with respect to the adjacent bottom layer. There is a slot in the ground-plane to couple the energy from the feed line to the dielectric resonators. The arrangement is such that the rectangular dielectric resonators are placed on the ground-plane with resonator 1 (upper dielectric layer) set to 48° for producing CP. The 2nd-order mode cannot be excited because it gets eradicated by the ground-plane. However, the fundamental and the 3rd-order modes, which look like TE111 mode and TE113 mode of grounded rectangular DRA can exist. This CP antenna yields 18.2% AR bandwidth at a center frequency of 5.5 GHz and an average gain of 4.5 dBi. The low profile of this antenna is a plus to be implemented in Wi-Fi and 5G applications.

A wideband CP DRA which is excited by an Archimedean spiral slot has proposed in [45]. The geometry of this antenna is depicted in figure 5. The antennas consist of a substrate with a complementary Archimedean slot and a rectangular dielectric resonator. The slot arms are terminated with two chip resonators. The antenna has fed by a coaxial cable located in the center of the spiral resonator. In order to realize a CP radiation, the two lowest broadsides which are TE_{111}^x and TE_{111}^y modes have used. This antenna has obtained a 3 dB AR bandwidth of 25.5% and a measured RHCP gain of 4.95 dBi at a center frequency of 2.11 GHz.

The other example which was used for MIMO feed is a T-shaped DRA [46]. This antenna contains a truncated ground-plane with a pair of microstrip-fed stubs printed on the lower side of a substrate, and a decoupling network on top of the substrate as shown in figure 6. CP for this particular structure is obtained by various orthogonal modes of excitation. The antenna can radiate LHCP and RHCP fields depending on port excitation since both ports lay on the same substrate si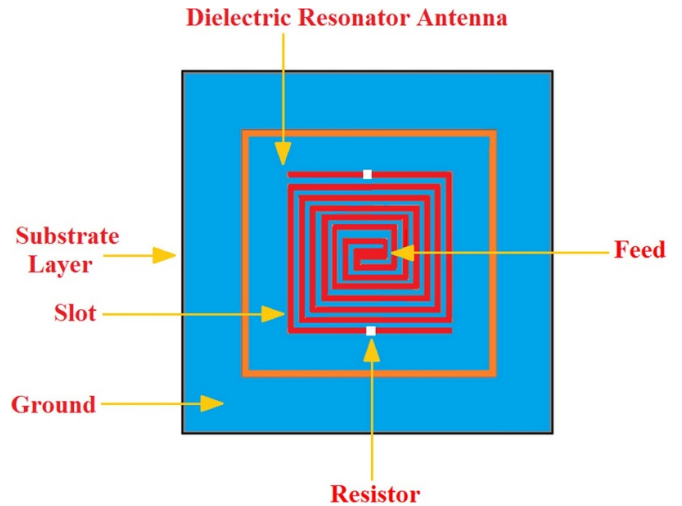de. The 1st and 2nd modes in the antenna are recognized as quasi-$TE_{11\delta}^x$ and quasi-$TE_{11\delta}^y$ $(0 < \delta < 1)$ with a phase of 90°. The isolation between ports increased to 22.5 dB by using the decoupling network. Basically, it greatly decreases the coupling energy between ports and enhances the radiated electric fields. High purity of the RHCP, compared with the LHCP, of more than 25 dB observed due to the truncated ground-plane and decoupling line under dielectric resonator of very high relative permittivity of 9.8. The antenna has realized a peak gain of 3.3 dBi and an operational bandwidth of 17.9% at an operation frequency band of 5.02–6.03 GHz.
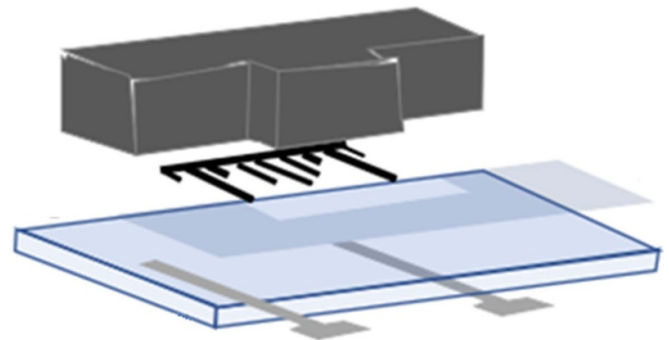
3.3. Reconfigurable CP antennas

Reconfigurable antennas have the capability of adapting radiation properties and frequency in a reversible and controlled manner [47, 48]. The switching mechanism is usually achieved through MEMS and optical switches, and varactor and PIN diodes to ON/CLOSE various antenna parts [49, 50]. Thus, printed reconfigurable antennas incorporate functional varieties. Moreover, they can provide diverse features of polarization, radiation pattern, and operating resonant frequency in 5G applications [51, 52].

J. Phys. D: Appl. Phys. **55** (2022) 033002

Topical Review

Three-layered substrate antenna composed of square radiator patch on top, L-shaped probes embedded with reconfigurable feeding network under top layer while the bottom side has dc biasing (mentioned as sub-DC) lines has presented in [25]. Since the square patch is excited by L-shaped probes, consequently the reconfigurability is attained by switching phase difference to clockwise/counter-clockwise of the PIN diodes in this feeding network. In order to switch between different modes of polarization, PIN diodes are used. Hence to control diodes voltage, a DC_1 connected with probes works for biasing radiating patch through RF chokes mentioned as pins P#1, P#2, and P#3. These probe pins work with the same amplitude and clockwise phase delay of 90°. Similarly, DC_2 is coupled with the $\lambda/4$ transformer of the feeding network. By altering the dc biasing, RHCP and LHCP radiations have realized. In this style, four plastic strew pieces and a 3D printed fixture have used to support antenna geometry. The current distribution of the RHCP mode at different time interval shows the achieved CP. The antenna yields a 28.8% AR bandwidth from 1.29 to 1.59 GHz for both polarizations. The measured peak gain value is 6.9 dBi.

A similar reconfigurable wideband CP antenna using an L-shaped feeding probe is reported in [53]. In this structure, the patch antenna has a square shape with two truncated corners to produce CP. The patch antenna is fed by the L-shaped probes and the L-shaped probes are connected to the matching circuits underneath of the ground-plane. The electrical switches consist of pin diodes and some RF/biasing components can provide the excitations for RHCP and LHCP for this antenna. The antenna yields a 20% AR bandwidth at the operating frequency band between 1.6 and 2.25 GHz and a gain of 5.6 dBi.

The other example of a reconfigurable CP antenna for MIMO feed antenna is a crossed Yagi patch antenna (CYPA) introduced in [52] which contains unique features of pattern reconfigurability. Two identical Yagi patch antennas with linear characteristics are arranged orthogonally along x- and y-axis to make it CP. The substrate's upper part has one driven and four parasitic square patches. However, to make it MIMO, the radiating patches are arranged in the form of arrays which share the driven patch by dual feed points organized on x- and y-axis known as x-feed and y-feed, respectively. The optimum distance of 5 mm is kept between two feeds to improve the impedance matching. When both feedings are excited simultaneously it produces radiation patterns. Both feeding points are operating at the specific phase shift resultant circularly polarized radiation pattern is achieved. The phase shift of 90° between two feed points improves AR, total co-polarization gain, and field gain. It means the x-feed is 90° advanced with respect to the y-feed, so the RHCP component was achieved. This covers the area between the directors of the two orthogonal arrays leads to extensive beam coverage improvement. In order to maintain CP performance, a 3 dB coupler is embedded with CYPA by sharing the same metal ground. Since patches are on the top side of the substrate, they are making layer-I, while the coupler on the bottom side forms layer-2.

Port-1 and port-4 (two SMA connectors) are the coupler input ports, while port-2 and port-3 are the coupler output ports fixed with a 90° phase shift further connected to the two feed points (x-feed and y-feed) by two probes, passed by two vias. Ground side expansion improves radiation patterns and impedance. As soon as coupler's port-1 is excited and port-4 is terminated with 50 Ω load, port-2 steered port-3 by 90°; hence, RHCP radiation pattern is achieved. Similarly, if port-4 is excited and port-1 terminated with a 50 Ω load, LHCP radiation pattern characteristics can be observed. In order to provide the characteristics of reconfigurability, ideal switch and simple MEMS switch models are incorporated into the CYPA. A composite slot composed of four x-axis rectangles and a narrow y-axis gap are printed in each parasitic patch's center. The closed (ON) or open (OFF) switch states generate many antenna modes due to variation in the equivalent inductance and capacitance of the patch. This CP antenna could achieve a peak gain of 8.68 dBi at an operating frequency range of 3.94–4.18 GHz.

3.4. SIW-CP antennas

SIW are planar structures fabricated by using periodic rows of either metallic vias (holes) or slots connecting top and bottom metallic ground-planes of a dielectric substrate [54–56]. It is an emerging approach to implement low-cost effective components, low loss antennas, and complete circuit systems at microwave and millimeter-wave frequencies [57, 58].

A novel feeding structured CP antenna composed of mainly three parts of a SIW based waveguide, a cavity-backed resonator, and a conventional ring-slot antenna is shown in [59]. This design accomplishes broadband impedance matching and RHCP generation by applying simple shorting among top patch and bottom ground-plane and by insertion of induction through arrays at the input port. The feeding waveguide of this design works at the cut-off frequency of 6.3 GHz and generates the fundamental TE_{10} mode. The leakage current at the sidewalls of the feeding waveguide is small. For high-speed data communication as required in 5G, this structure can be used in a phased array antenna.

The other CP SIW antenna is a miniaturized CP antenna with TE_{10}-mode [60]. The geometry of the antenna is shown in figure 7. In this structure, two 1/8 of SIW cavities are placed orthogonally to produced CP with a dominant TE_{10}-mode. As a result, a significant size reduction has been achieved. Besides that, due to via wall the cavities could be placed very closed to each other. The two cavities are needed to be excited with electromagnetic fields with equal magnitude and 90° phase shift. This excitation is produced using a quadrature-coupler. The antenna produces a 3 dB AR bandwidth between 1.64 and 1.65 GHz and a measured peak gain of 2.3 dBi at 1.645 GHz.

Another example of a wideband CP SIW end-fire antenna with dual ports viewed as a two-element array having a single layer structure is depicted in figure 8 [61]. Two orthogonally polarized end-fire elements with wave-rotation in planar SIW structure are used. The horizontally polarized (HP) element is SIW antipodal tapered slot antenna, while the vertically polarized (VP) element employed is an open-ended SIW radiator with the printed transition. These HP and VP elements fed by SIW narrow-wall 90° directional coupler satisfy CP wave requirement. The design ensures the existence of the
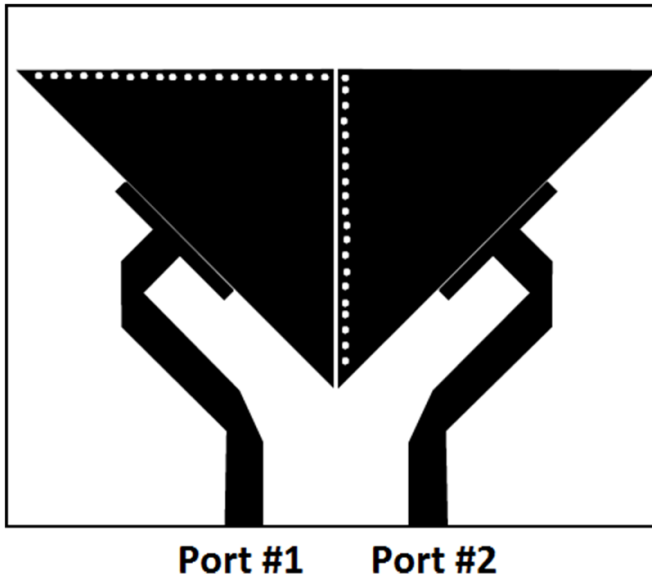
Figure 7. Configuration of miniaturized CP antenna based on SIW. © 2014 IEEE. Reprinted, with permission, from [60].
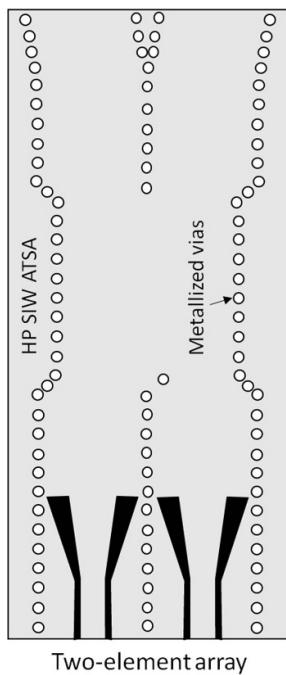

Figure 8. CP SIW end-fire antenna with dual ports viewed as a two-element. John Wiley & Sons. © 2017 Wiley Periodicals, Inc.

fundamental TE_{10}-mode. The dimensions include two rows of metalized vias consisting of 0.8 mm diameter and pitch size (center-to-center spacing) of 1.6 mm, resulting in the narrow walls of the open-ended SIW radiator.

3.5. Fractal CP antennas

Fractal antennas have realized as multilevel structures, space-filling small curves, self-symmetry, or analogous geometries

to increase the effective length and maximize the perimeter of the antennas [62, 63]. In general, it is considered as a suitable method to attain 50%–75% of practical shrinking while maintaining performance level very high and efficient. Therefore, for applications in which small size embedded antenna and transparent materials to realize near-invisible form factors fractal antennas can be used [64, 65]. Generally speaking, the fractal curve is fickle, e.g. Sierpinski, Koch.

Wunderlich-shaped fractal complementary split-ring resonator (WCSRR) in designing CP antenna by combining CSRR and fractal strategy has presented in [66]. Moreover, Hilbert-shaped reactive impedance surface (HRIS) has upgraded the front-to-back ratio and substrate thickness. This is known as HRIS-inspired WCSRR-loaded CP antenna. The radiating patch is over the HRIS layer and an asymmetrical microstrip feeding stub improves AR. WCSRR etched on the radiating patch expands geometrical compactness and also orthogonal modes excitation with 90° phase difference. Overall, this fractal CP antenna contains two dielectric substrates of various dimensions. In order to reduce stochastic and mechanical errors during the assembling process, HRIS cells and the radiating patch are fabricated on the top sides of both substrates. However, these identical footprinted substrate layers are tightly boned together by an adhesive material by going through a hot press. Based on the given time-domain E-field distribution at 3.5 GHz, which is presented in [66], there is an electric field clockwise rotation along the edge of the radiating patch that demonstrates strong LHCP. However, RHCP characteristics can be acquired by mirroring the WCSRR structure on the top right side of the radiating patch. Additionally, the divergence of the electric field along WCSRR at different time stages ($t = 0$, $T/8$, $3T/8$, $T/4$) indicates the importance of CSRR in CP wave excitation. This strategy's noticeable improvements are that it does not require any (a) sophisticated feeding networks, (b) metallic via or holes, and (c) truncated corners of arbitrary shape.

The other CP antennas with fractal structures are a single feed compact annular slot antenna loaded with diagonal slots [67] (see figure 9(a)) and fractal fork slot antennas [68] (see figure 9(b)). In the first structure exhibited in figure 9(a) a set of fractal slots diagonally caused a perturbation to produce orthogonal degenerate mode. While the 2nd fork fractal slot antenna displayed in figure 9(b) utilizes an inverted L-shaped monopole with a 3rd iterative fractal slot in the ground-plane to produce CP. The circular fractal antenna yields 21% AR bandwidth and a measured peak gain of 6.6 dBi at 1.775 GHz. And the fork fractal antenna provides a 15.5% AR bandwidth at a center frequency of 2 GHz and a gain between 2 to 5 dBi.

A MIMO fractal antenna with dual radiation elements and CP having low mutual coupling is shown in [69]. Each radiating element is configured using a semi-crescent structure (SC1, SC2, SC3) scaled down in a cascade arrangement making each shape like the scorpion tail. In order to reduce the mutual coupling, the location of antennas is in close proximity to the right and left edges. For both elements at 1.5 and 5 GHz the LHCP and RHCP radiation patterns have the phase difference of 35° and 170°, and at 2.7 and 3 GHz radiation patterns are shifted by 85°, i.e. nearly perpendicular to each other.
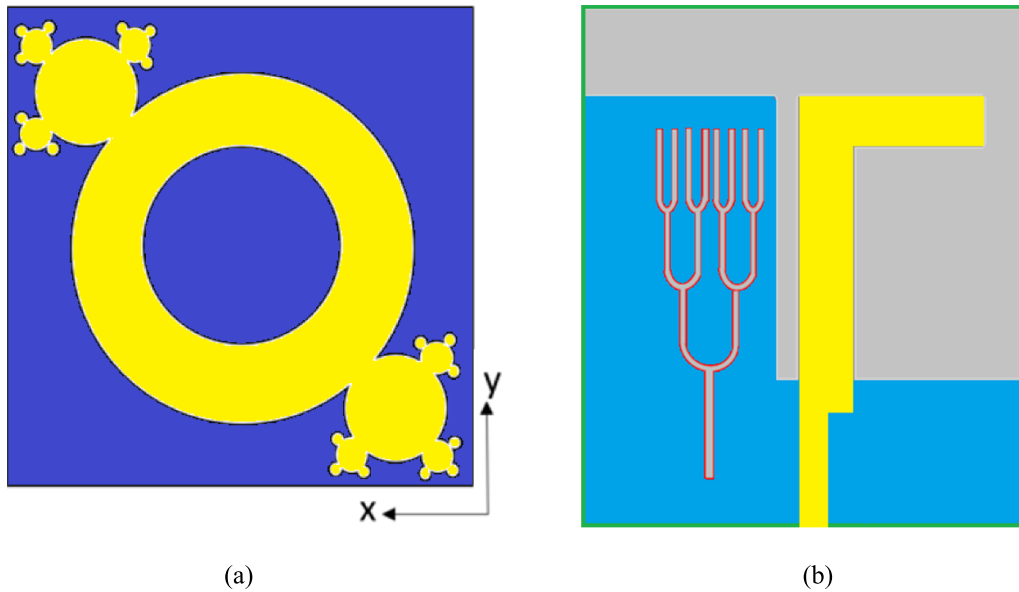
Figure 9. (a) Geometry of annular slot antenna with diagonal slots (© 2015 IEEE. Reprinted, with permission, from [67]) and (b) geometry of fork fractal slot antenna (reproduced from [68]. CC BY 4.0).

Based on the distribution of surface current at three phases, it is clear that when the phase changes the surface current's direction also changes sequentially. As a result, two current components perpendicular to each other generate two normal electric fields required for CP generation.

3.6. Hybrid techniques CP antennas

Figure 10 shows the geometry of a cavity-backed CP antenna consists of two crossed strip dipoles, an asymmetrical cross loop, two vacant-quarter phase delay rings, a metal cavity, and a semi-rigid coaxial cable. The antenna is encircled by a novel asymmetrical cross-loop [70]. Both sides of the substrate comprise of symmetrical pair of vacant-quarter rings and crossed dipoles. The cross-loop is printed on top of the substrate, and it encircles the crossed dipole with a specific space parameter. As exhibited in figure 10 an air gap of 2.3 mm is arranged to make cross-loop work like a spiral, as in [71]. The main purpose of this cross-loop is to differentiate two orthogonal electric field E-components for CP wave realization. A metal cavity is placed underneath the substrate at a distance of 16 mm to visualize a unidirectional radiation pattern. This distance is estimated from quarter-wavelength at the center frequency of CP bandwidth. A semi-rigid coaxial cable is punctured through the bottom cavity. The antenna provides a 3 dB AR bandwidth of 1.39–1.82 GHz, a maximum gain of 8.3 dBi and a high radiation efficiency within the operational bandwidth. Similarly, a dual-polarized dual-band omni-directional antenna consists of a circular patch with eight open slots, eight shorted metal pins, and a central feed coaxial probe has presented in [72].

The other example is an artificial magnetic conductor (AMC) reflector [73] based antenna consists of a crossed dipole [74, 75] and a Γ-shaped 90° phase shifter feed network (Wilkinson power divider [76]). AMC cells are printed
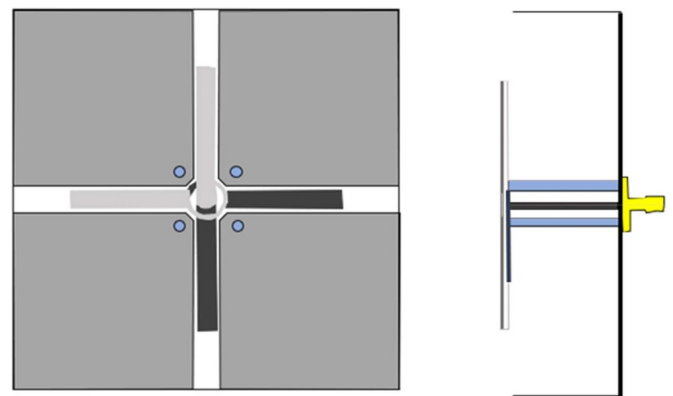

Figure 10. Geometry of crossed dipole loaded with magneto-electric dipole, left- and right-sides represent the top- and side-views. © 2015 IEEE. Reprinted, with permission, from [71].

on the upper side of FR4 while the feed network is implemented on the lower substrate side. The ground patch coincides with the crossed dipole feeder and output ports of 90° feed network through the AMC reflector. In order to avoid short-circuiting two small square gaps are added on the ground-plane. The excitation through the feed network divides into two signals with equal amplitude and phase difference of 90°, hence the cross dipole also gets excited and CP radiation is achieved. This crossed dipole is etched over vertical substrate connected through radiation patches. Moreover, two rectangle patches printed on the other side of the substrate are also connected to the radiation patches and shorted the ground. This printed dipole can be considered to be fed by a slot line that is coupled to microstrip lines on the one hand and extended to a shorted stub on the other hand [77]. This broadband crossed-dipole antenna is suitable to achieve a wideband 1.19–2.37 GHz (66.3%), if CP antenna it is fed by a 90° shifter. The

AR bandwidth <3 dB is about 1.25–1.97 GHz (44.7%). Hence, the antenna has very low profile of 20.1 mm (about $0.12\lambda_0$ at the center frequency of 1.78 GHz).

3.7. 3D-printing CP antennas

3D printing technology is opening innovative abilities and prospects to complex antenna geometries [78]. It also enables an extraordinary level of correctness, efficiency and eases the fabrication process, especially for non-planar, flexible, and volumetric structures [79, 80]. Difficult to fabricate geometries are now possible that can result in new antenna functionalities and extended performance (e.g. lower frequency resonance in small volumes, wider bandwidth, narrow-beam directionality). Producing CP antennas using 3D printing techniques has gained so much traction in recent years as reported in [81–84]. In general, there are processes, such as laser melting, binder jetting, and plated vat photopolymerization [85], that provide advantages in term of mechanical and electromagnetic performance but are very rare found in the fabrication of CP antennas. There is now an increased interest in additive manufacturing (AM) [86, 87] in microwave community as it offers customization, design freedom and potential cost reduction especially in low volume productions. Moreover, now available is layer by layer fabrication of dielectric and metals using fuse deposition modeling (FDM) [88] and stereolithography (SLA) [89]. Metallic layers are easily added on substrates using FDM, where a dispenser is required to add layers of silver conductive pastes. The problem with FDM substrates is the roughness of the surfaces, which limits the thickness of metallic layers since it is paste based. On the other hand, SLA based substrates provides a smoother surface finish. There is also an advantage when fabricating with other types of metallic layer deposition processes such as inkjet printing [90].

Four arms helix antenna (quadrifilar) manufactured through 3D printer has shown in figure 11 [91]. Two approaches are used to miniaturize the antenna structure. Initially, circular conductive disks are loaded by the tips of the four helical arms as exhibited in figure 11(a). These arms are circumferentially equally spaced along with the cylinder and are positioned in such a way that their relevant centers are connected to the tip of those arms. Helix diameter, spacing among each arm, turn number, wire diameter, phase difference, and ground-plane dimension manage the operation of a quadrifilar helix antenna. Moreover, a cone inner radius of 3 cm is used to accommodate the four feeding connectors to the arms during testing. Whereas the 2nd approach is based on the integration of dielectric material into the vacant space between the quadrifilar helix arms as displayed in figure 11(b). Each arm is fixed at the helix angle of 73°, and clockwise direction winding on each arm is used. Further, the addition of dielectric slabs slows down the effect of traveling waves along with helical arms results improvement in the resonant frequency. At the final stage shown in figure 11(c), ground-plane changed to the cone-shaped ground (modeled into conical shape) gives a positive impact. It increases gain, directivity, and antenna structure compactness. During fabrication, each helical arm is printed

using a laser-based technique. Polyactic acid dielectric material of relative permittivity of 3.1 and adhesive copper wrappings are also used. Moreover, conductive paint is sprayed on the plastic arms and electroplated. Both methods make quadrifilar to produce excited current along the continuous path. Quadrifilar helix antennas are useful for mobile terminals in satellite communications.

The other example of 3D printed is a CP antenna circular radiation patch with a crossed slot with high efficiency and wide beamwidth [84]. The antenna consists of a radiation PCB, a feed cylinder, and a network PCB. The components are integrated without any additional supporting structure. In this antenna, the cross-slot is used to improve the impedance matching as well as to reduce the size by splitting the antenna into four radiation sectors connected to triangular feed patches. The purpose of the triangle fed patches and the no-resistor series feed line are to increase the bandwidth, and efficiency, respectively. The bottom four patches are excited with the same amplitude and −90° phase differences to produce CP. The antenna yields an AR bandwidth of 8.3%, a gain of over 5.2 dBi, and an efficiency of more than 95%.

In addition, a 3D-printed unidirectional wideband antenna, based on two crossed magnetoelectric (ME) dipoles has presented in [92]. It comprises of folding the electrical dipole elements; thus, each dipole arm is prototyped using 3D printing technology. The antenna contains four horizontally folded square loops operating together as two crossed electric dipoles. Vertical plates are used for the shortening of each horizontal plate to the ground-plane. Every adjacent vertically oriented plate acts like a magnetic dipole and generates dual polarization at 0° and 90°. Two Γ-shaped strips are orthogonally placed in the gaps between the vertical plates. These Γ-shaped excitation strips are erected using three slices of the double-sided RT5870 substrate-PC. Port-1 is the lower strip, and port-2 is the higher strip. Shorter and higher strips excite 90° and 0° polarization, respectively. However, for the improvement in radiation characteristics ME dipoles are mounted on a square cavity. For the reduction of volume, the electric dipole from square plates transformed into folded square loops. 3D printed technology with plastic material electroplated with copper. Furthermore, CP has been generated by adding a 90° hybrid coupler circuit IPP-7026. This coupler was mounted on a PC and a metallic test board and connected to antenna ports using two equi-phased semi-rigid RF cables. Antenna miniaturization can be achieved by increasing the current path length of electric dipoles.

CP antennas based on inkjet printing is reported in [93] for global positioning system (GPS) applications. This antenna consists of a planar monopole where an L-shaped slit is used to transform it to exhibit circularly polarized characteristics. The slit divides the current distribution on the monopole in two orthogonal directions with necessary phase shifts. This results from the unequal lengths of the slits. The gap between the monopole and the ground-plane helps in the impedance matching by providing a capacitive loading which makes the inductive impedance of the monopole achieve close to real impedance of 50 Ω. Here Kodak photo paper is used as substrate. The antenna is shown to provide a gain of 0.2 dBi at 1.575 GHz
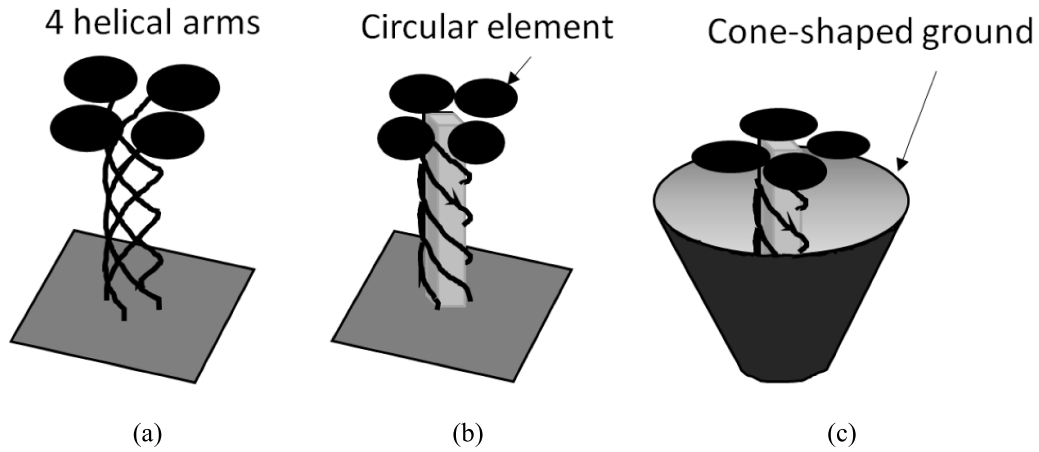
Figure 11. Quadrifilar helix antenna: (a) four helical arms, (b) circular element, and (c) cone-shaped ground. © 2017 IEEE. Reprinted, with permission, from [91].
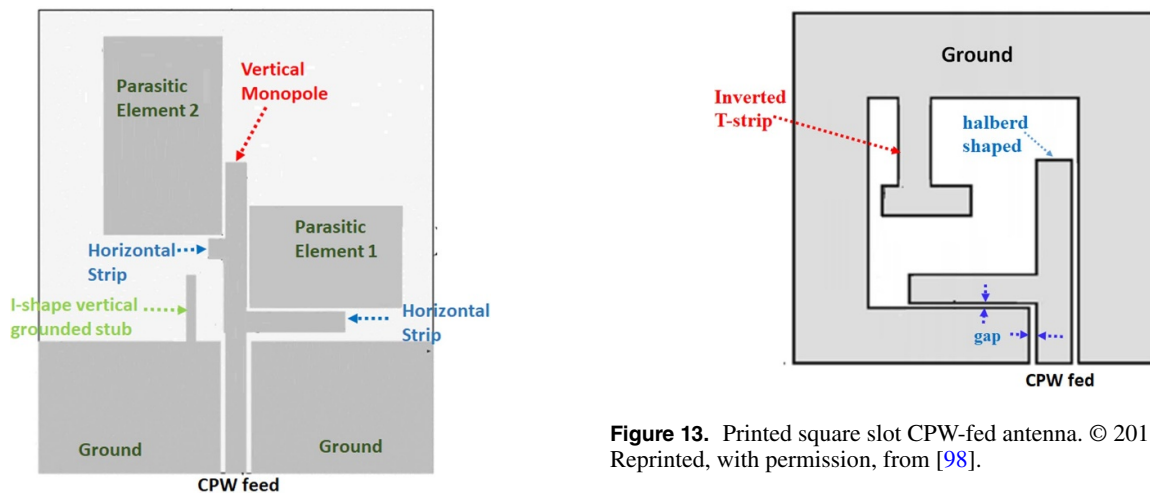

Figure 12. CPW-fed dual-band printed monopole CP antenna. © 2017 IEEE. Reprinted, with permission, from [98].

Figure 13. Printed square slot CPW-fed antenna. © 2011 IEEE. Reprinted, with permission, from [98].

with 3 dB AR bandwidth of 3.8%. In [94] a circularly polarized patch antenna design is shown which is conformal to a cylindrical surface. By cutting the two bottom corners of the GPS patch results in the generation of two orthogonal modes with a phase shift of 90°. The antenna is excited via the coupling from the T-shaped feedline. It is found that by wrapping the antenna around a cylindrical surface the width of the antenna will need to be adjusted to maintain the CP. Here polycarbonate was used as the antenna substrate since it is easy to be wrapped around a cylindrical structure. The thickness of the substrate is 1.524 mm and it had a permittivity of 2.9. The antenna was manufactured using the inkjet printing method using conductive ink, which was placed on a transparency, and then the transparency was taped on the payload. The manufacturing equipment used comprised (a) an Epson C88+ printer, (b) conductive ink Metalon JS-B525P from Novacentrix, and (c) Novele™ coated polyethylene terephthalate transparencies. Thickness of the ink is typically between 500 and 1000 nm. This antenna had RHCP reasonable (AR) operating at 2.225 GHz.

Similarly, in [83] CP patch antenna is manufactured by combining inkjet printing and SLA technology. The substrate was fabricated by curing photosensitive resin, and inkjet printing was used to fabricate the patch element by utilizing silver ink.

3.8. CPW-CP antenna

Classic CPW [95] is a conductor separated from a pair of ground-planes implemented on the same top side plane of a dielectric medium. In an ideal case the thickness of the dielectric medium is infinite, however, in practice the thickness is made sufficient for EM fields to pass through the finite substrate [96]. A variant of CPW is formed when a ground-plane is provided on the opposite side of the dielectric, which is commonly referred to as finite ground-plane CPW or grounded CPW [97].

Figure 12 shows the CPW-fed dual-band printed monopole CP antenna [98]. The basic antenna contains a vertical monopole with two horizontal stripes on both sides. The width of horizontal strip is the same as of the vertical branch. The structure provides two components of electric currents in orthogonal directions. Length of the horizontal strip is a quarter

Table 1. Comparison between the characteristics of CP antennas discussed in this survey.

Reference	Design approach	Novelty	Operating frequency	AR bandwidth	Feed type	Gain
[25]	Reconfigurable	L-shaped feeding probes and pin diode	1.39 GHz	28.8%	Single	6.9 dBi
[31]	Printed CP array of 5 × 5	Corner-truncated patch, sequential rotated four parasitic strips and gap-coupled around the patch	2.4 GHz	8.1%	Single	9.3 dBi
[33]	—	A capacitive feeding and an upper parasitic notched patch	5 GHz	10%	Single	6 dBi
[36]	Printed CP 2 × 2	Slot antenna with spline curves and phase shifter	4.6 GHz	54%	Dual	1.6 dBi
[39]	Dielectric resonator	DRA employing rotated-stair dielectric resonator	5.5 GHz	18.2%	Single	4.5 dBi
[40]	DRA	T-shaped dielectric resonator	5.52 GHz	17.39%	Dual	3.3 dBi
[45]	DRA	Archimedean slot excitation	2.11 GHz	25.5%	Single	4.95 dBi
[46]	Reconfigurable	Crossed-Vagi patch	4.06 GHz	5.9%	Dual	8.68 dBi
[53]	Reconfigurable	L-shaped fed and electrical switches	1.925 GHz	20%	Single	5.6 dBi
[60]	SIW	Miniaturized structure with dominant TE_{10} mode	1.645 GHz	12%	Single	2.3 dBi
[62]	Hybrid	Cavity-backed	1.6 GHz	26%	Single	8.3 dBi
[67]	Fractal	Annular slot antenna with diagonal slots	1.775 GHz	21%	Single	6.6 dBi
[68]	Fractal	Fork slot	2 GHz	15.5%	Single	2–5 dBi
[84]	3D printed	Crossed slots and cylindrical feed	1.2 GHz	8.3%	Single	5.2 dBi

of a guided wavelength at 2.6 GHz. However, vertical strip's length is more than 1/4 of a guided wavelength, but less than half of a guided wavelength at 2.6 GHz. Thus, input current in the horizontal branch is in phase to its input voltage as it acts as a series resonator. Conversely, input current in vertical branch lags the input voltage by 90° as the input impedance is inductive. Therefore, *X*-directed horizontal current leads the *Y*-directed vertical current by 90°. This results in RHCP. The input impedance, and hence the current in vertical branch, can be tuned by its length. Thus, the length of the vertical strip is adjusted to obtain equal magnitude of current on both the branches. Added on either side of the vertical monopole are parasitic elements to realize wideband impedance matching. Two parasitic elements are placed adjacent to each horizontal branch. The gap between parasitic elements and monopole is 0.5 mm. To improve the AR over the upper band, an I-shape vertical grounded stub needs to be added. This provides 3 dB AR fractional bandwidth of 27.45% at 2.55 GHz (RHCP) and 7.1% at 3.53 GHz (LHCP). Similar characteristics can be seen in [99]. These types of antennas can be used for GPS remote sensing applications.

As another example of printed square slot antenna fed by a CPW is presented in figure 13 [100, 101]. In this antenna the 3 dB AR band is enhanced by extending the feedline leftward along the *X*-direction and upward along the *Y*-direction to form a halberd-shaped structure. The impedance band is improved by implanting within the slot a grounded asymmetric inverted-T strip [101]. The position of the CP band can be controlled by varying the length and width of halberd-shaped feedline. This antenna is shown to provide a 3 dB ARBW of 3.81% over its impedance band with a maximum gain of 1.8 dBi.

4. State-of-the-art comparison

In this section, a comprehensive comparison is provided of the CP antenna examples discussed above in terms of design approach, novelty, operating frequency, AR bandwidth, feed type, and gain. Table 1 shows the various techniques utilized to date to realize CP antennas. The CP antenna designs presented in [25, 31, 33, 39, 45, 53, 60, 62, 67, 68, 84] are suitable for single port antennas, and while the other designs introduced in [36, 40, 46] are applicable for dual port antennas. The operating frequency of all antennas cited in the table is in the range of 1.2–5.5 GHz.

The use of reconfigurable antennas for 'green' and flexible 5G systems operating between 3.4 and 3.8 GHz are becoming

popular [102]. Interest in reconfigurable antennas is driven by the need for wireless systems that combine multiple standards and for the need to build systems with a small form factor [103].

Among the listed CP antennas in this table, the proposed printed antenna in [31], reconfigurable antenna in [46], and hybrid antenna in [62] show the highest gain of 9.3, 8.68, and 8.3 dBi, respectively, compared to others. While the CP antennas introduced in [25, 36, 45, 62], which are based on the reconfigurable, printed, DRA, and hybrid methods provide AR bandwidth of 28.8%, 54%, 25.5%, and 26%, respectively, which are larger than other CP antennas in table 1. In [94], the impedance matching is offset by the air gap between the patch and the substrate. As the antenna structures get complex, the conventional layering technique used to fabricate antennas increase the possibility of manufacturing errors that can affect the performance of the antenna. However, with the 3D printing technology available today it is possible to fabricate antennas to a high degree of accuracy.

5. Conclusion

This survey has investigated CP single and MIMO techniques by considering their use in the design of antennas presented in the available literature. To analyze the critical features of CP theory and concept several examples have used. Comparisons on the basis of design approach, novelty, operating frequency, AR bandwidth, feed type, and gain are made for all the examples. The fundamental information on RHCP and LHCP surveyed here is a prerequisite for moving further along the road to 5G and mmWave applications. Additionally, further research is going on to develop such CP antennas that gives enhanced AR bandwidth and gain. So it will be possible to use only CP antennas for mobile communication since the LP antennas include many drawbacks. If the CP antennas meet the requirement of long-distance mobile communication as done by high gain linearly polarized antennas, they could become major technology and there will be a remarkable reduction in number of LP antennas required for mobile telecommunications. Ultimately, they can save the cost of installing number of LP antennas, and the mobile users have to pay the minimum cost to service providers available. Thus, the development of proper CP antenna models (designs) are vital, not only for the long-term development of future mmWave wireless communication systems applications but also for a fundamental understanding of students, scholars, and future engineers who want to work, improve and develop mobile industry. Hence, a broad range of CP antenna design possibilities is introduced in this review study to highlight the improvement of their performance parameters that is rare in the available literature.

Data availability statement

All data that support the findings of this study are included within the article (and any supplementary files).

Institutional review board statement

Not applicable.

Informed consent statement

Not applicable.

Conflicts of interest

The authors declare no conflict of interest.

ORCID iDs

Iram Nadeem https://orcid.org/0000-0001-6635-343X
Mohammad Alibakhshikenari https://orcid.org/0000-0002-8263-1572
Ayman A Althuwayb https://orcid.org/0000-0001-5160-5016
Isabelle Huynen https://orcid.org/0000-0002-8504-2896

References

[1] Counselman C C 1999 Multipath-rejecting GPS antennas *Proc. IEEE* **87** 86–91

[2] Pancera E 2010 Medical applications of the ultra wideband technology *Loughborough Antennas Propagation Conf.* pp 52–56

[3] Chávez-Santiago R, Balasingham I and Bergsland J 2012 Ultrawideband technology in medicine: a survey *J. Electr. Comput. Eng.* **2012** 1–9

[4] Toh B Y, Cahill R and Fusco V F 2003 Understanding and measuring circular polarization *IEEE Trans. Educ.* **46** 313–8

[5] Sichak W and Milazzo S 1948 Antennas for circular polarization *Proc. IRE* **36** 997–1001

[6] Rashid K A A *et al* 2014 A review on circular polarization antenna for wireless MIMO application *Int. Symp. on Technology Management and Emerging Technologies* pp 73–77

[7] Li L, Li J, He B, Zhang S and Zhang A 2016 A compact circularly polarized microstrip antenna with bandwidth enhancement *Prog. Electromagn. Res.* **61** 85–89

[8] Hubka P and Lacik J 2016 X-band circularly polarized HMSIW U-slot antenna *Radioengineering* **25** 687–92

[9] Sze J and Chen W 2011 Axial-ratio-bandwidth enhancement of a microstrip-line-fed circularly polarized annular-ring slot antenna *IEEE Trans. Antennas Propag.* **59** 2450–6

[10] Takeshi M, Sato K, Masuzawa H, Taira K, Ihara T, Kasashima Y and Yamaki K 1995 Polarization dependence

of multipath propagation and high-speed transmission characteristics of indoor millimeter-wave channel at 60 GHz *IEEE Trans. Vehicular Technol.* **44** 268–74

[11] Abadi S M A M H and Behdad N 2016 Wideband linear-to-circular polarization converters based on miniaturized-element frequency selective surfaces *IEEE Trans. Antennas Propag.* **64** 525–34

[12] Huang J 1986 A technique for an array to generate circular polarization with linearly polarized elements *IEEE Trans. Antennas Propag.* **34** 1113–24

[13] Chang T N 2009 Circularly polarized antenna for 2.3–2.7 GHz WiMax band *Microw. Opt. Technol. Lett.* **51** 2921–3

[14] Ahn J-S, Ha D-H and Cho P-D 2006 The circular polarization diversity effect considering XPD factor in an indoor radio propagation environment *J. Electromagn. Eng. Sci.* **6** 24–29

[15] Xie L, Cui X, Zhao S and Lu M 2017 Mitigating multipath bias using a dual-polarization antenna: theoretical performance, algorithm design, and simulation *Sensors* **17** Feb

[16] Mishra P K, Jahagirdar D R and Kumar G 2014 A review of broadband dual linearly polarized microstrip antenna designs with high isolation [education column] *IEEE Antennas Propag. Mag.* **56** 238–51

[17] Wang J, Lv Z and Li X 2014 Analysis of MIMO diversity improvement using circular polarized antenna *Int. J. Antennas Propag.* **2014** 570923

[18] Kellomäki T 2012 Analysis of circular polarization of cylindrically bent microstrip antennas *Int. J. Antennas Propag.* **2012** 858031

[19] Ram K R V S and Kumar R 2013 Design of ultra-wideband trapezoidal shape slot antenna with circular polarization *AEU-Int. J. Electron. Commun.* **67** 1038–47

[20] Hurd G A 1980 IEEE standard test procedures for antennas *Electron. Power* **26,** 749

[21] Dunn D S and Augustin E P 1993 Technique measures gain for different antenna polarizations *Microw. RF* **32** 94

[22] de Jough R V, Hajian M and Ligthart L P 1997 Antenna time-domain measurement techniques *IEEE Antennas Propag. Mag.* **39** 7–11

[23] Lo Y T 1993 *Antenna Handbook: Antenna Fundamentals and Mathematical Techniques* (New york: Springer Science & Business Media)

[24] Sun L, Ou G, Lu Y, Shusen T and Kishk A 2013 Axial ratio bandwidth of a circularly polarized microstrip antenna *Advancement in Microstrip Antennas with Recent Applications* (Rijeka: InTech) pp 229–46

[25] Lin W and Wong H 2017 Wideband circular-polarization reconfigurable antenna with L-shaped feeding probes *IEEE Antennas Wirel. Propag. Lett.* **16** 2114–7

[26] Zhou P, Zhang Z, He M, Hao Y and Zhang C 2018 Design of a small-size broadband circularly polarized microstrip antenna array *Int. J. Antennas Propag.* **2018** 1–10

[27] Fu S, Fang S, Wang Z and Li X 2009 Broadband circularly polarized slot antenna array fed by asymmetric CPW for L-band applications *IEEE Antennas Wirel. Propag. Lett.* **8** 1014–6

[28] Yang S S, Kishk A A and Lee K 2008 Wideband circularly polarized antenna with L-shaped slot *IEEE Trans. Antennas Propag.* **56** 1780–3

[29] Huang J, Qiu F, Lin W, Tang Z, Lei D, Yao M, Chu Q X and Guo Y J 2017 A new compact and high gain circularly-polarized slot antenna array for Ku-band mobile satellite TV reception *IEEE Access* **5** 6707–14

[30] Chen H M, Chiu K Y, Lin Y F and Yeh S A 2012 Circularly polarized slot antenna design and analysis using magnetic

current distribution for rfid reader applications *Microw. Opt. Technol. Lett.* **54** 2016–23

[31] Wu J, Yin Y, Wang Z and Lian R 2015 Broadband circularly polarized patch antenna with parasitic strips *IEEE Antennas Wirel. Propag. Lett.* **14** 559–62

[32] Chang T-N and Jiang J-H 2009 Enhance gain and bandwidth of circularly polarized microstrip patch antenna using gap-coupled method *Prog. Electromagn. Res.* **96** 127–39

[33] Guo Y-X and Tan D C H 2009 Wideband single-feed circularly polarized patch antenna with conical radiation pattern *IEEE Antennas Wirel. Propag. Lett.* **8** 924–6

[34] Deng C, Li Y, Zhang Z, Pan G and Feng Z 2013 Dual-band circularly polarized rotated patch antenna with a parasitic circular patch loading *IEEE Antennas Wirel. Propag. Lett.* **12** 492–5

[35] Fu S, Kong Q, Fang S and Wang Z 2014 Broadband circularly polarized microstrip antenna with coplanar parasitic ring slot patch for L-band satellite system application *IEEE Antennas Wirel. Propag. Lett.* **13** 943–6

[36] Narbudowicz A, John M, Sipal V, Bao X and Ammann M J 2015 Design method for wideband circularly polarized slot antennas *IEEE Trans. Antennas Propag.* **63** 4271–9

[37] Thomas K G and Praveen G 2012 A novel wideband circularly polarized printed antenna *IEEE Trans. Antennas Propag.* **60** 5564–70

[38] Zhou S W, Li P H, Wang Y, Fend W-H and Liu Z-Q 2011 A CPW fed broadband circularly polarized regular-hexagonal slot antenna with L-shape monopole *IEEE Antennas Wirel. Propag. Lett.* **10** 1182–5

[39] Pourahmadazar J, Ghobadi C, Nourinia J, Felegari N and Shirzad H 2011 Broadband CPW-fed circularly polarized square slot antenna with inverted-L strips for UWB applications *IEEE Antennas Wirel. Propag. Lett.* **10** 369–72

[40] Petosa 2007 *Dielectric Resonator Antenna Handbook* (Norwood, MA: Artech House)

[41] Wee F H, Malek M F B A, Sreekantan S, Al-Amani A U, Ghani F and You Y K 2011 Investigation of the characteristics of barium strontium titanate (BST) dielectric resonator ceramic loaded on array antennas *Prog. Electromagn. Res.* **121** 181–213

[42] Leung K W and Ng H K 2003 Theory and experiment of circularly polarized dielectric resonator antenna with a parasitic patch *IEEE Trans. Antennas Propag.* **51** 405–12

[43] Mongia R K and Ittipiboon A 1997 Theoretical and experimental investigations on rectangular dielectric resonator antennas *IEEE Trans. Antennas Propag.* **45** 1348–56

[44] Wang K X and Wong H 2015 A circularly polarized antenna by using rotated-stair dielectric resonator *IEEE Antennas Wirel. Propag. Lett.* **14** 787–90

[45] Zou M, Pan J and Nie Z 2014 A wideband circularly polarized rectangular dielectric resonator antenna excited by an archimedean spiral slot *IEEE Antennas Wirel. Propag. Lett.* **14** 446–9

[46] Lu L, Jiao Y C, Liang W and Zhang H 2016 A novel low-profile dual circularly polarized dielectric resonator antenna *IEEE Trans. Antennas Propag.* **64** 4078–83

[47] Huff G H and Bernhard J T 2007 Reconfigurable antennas *Modern Antenna Handbook* (Hoboken, NJ: Wiley-Blackwell) pp 369–98 (Accessed 26 November 2007)

[48] Jiajie Z, Anguo W and Peng W 2008 A survey on reconfigurable antennas *Int. Conf. Microw. Millim. Wave Technol.* **3** 1156–9

[49] Kholapure S and Karandikar R G 2016 Emerging techniques for printed reconfigurable antenna: a review *Second Int.*

J. Phys. D: Appl. Phys. **55** (2022) 033002

Topical Review

Conf. on Research in Computational Intelligence and Communication Networks (ICRCICN) pp 57–61

[50] Costantine J, Tawk Y and Christodoulou C G 2016 Reconfigurable antennas *Handbook of Antenna Technologies* ed Z N Chen, D Liu, H Nakano, X Qing and T Zwick (Singapore: Springer Singapore) pp 1737–72

[51] Bai Y, Xiao S, Liu C, Shuai X and Wang B 2013 Design of pattern reconfigurable antennas based on a two-element dipole array model *IEEE Trans. Antennas Propag.* **61** 4867–71

[52] Yang X, Wang B, Yeung S H, Xue Q and Man K F 2011 Circularly polarized reconfigurable crossed-Yagi patch antenna *IEEE Antennas Propag. Mag.* **53** 65–80

[53] Yang S S and Luk K 2006 A wideband circularly polarized reconfigurable patch antenna excited by L-shaped probes *2006 Asia-Pacific Microwave Conf.* (IEEE) pp 81–84

[54] Rayas-Sanchez J E and Gutierrez-Ayala V 2008 A general EM-based design procedure for single-layer substrate integrated waveguide interconnects with microstrip transitions *2008 IEEE MTT-S Int. Microwave Symp. Digest* pp 983–6

[55] Bozzi M, Perregrini L, Ke W and Arcioni P 2009 Current and future research trends in substrate integrated waveguide technology *Radioengineering* **18** 201–9

[56] Bozzi M 2012 Substrate integrated waveguide (SIW) technology: new research trends for low-cost and eco-friendly wireless systems *IEEE MTT-S Int. Microwave Workshop Series on Millimeter Wave Wireless Technology and Applications* pp 1–1

[57] Dahiya A, Sengar A P S, Dwivedi D K and Kumar A 2016 A critical review of substrate integrated waveguide for microwave applications *Second Int. Conf. on Computational Intelligence Communication Technology (CICT)* pp 495–9

[58] Dia'aaldin J B, Liao S and Xue Q 2015 High gain and low cost differentially fed circularly polarized planar aperture antenna for broadband millimeter-wave applications *IEEE Trans. Antennas Propag.* **64** 33–42

[59] Kim D, Lee J W, Cho C S and Lee T K 2009 X-band circular ring-slot antenna embedded in single-layered SIW for circular polarisation *Electron. Lett.* **45,** 668–9

[60] Kim K and Lim S 2014 Miniaturized circular polarized TE10-mode substrate-integrated-waveguide antenna *IEEE Antennas Wirel. Propag. Lett.* **13** 658–61

[61] Cai Y, Zhang Y, Yang L and Qian Z 2017 A low profile circularly polarized SIW end-fire antenna incorporating orthogonally polarized elements *Microw. Opt. Technol. Lett.* **59** 1111–5

[62] Ahmed E O and Jamal Z 2016 Handbook of research on advanced trends in microwave and communication engineering *IGI Global* 25 August 2016

[63] Anguera J, Puente C, Borja C and Soler J 2005 Fractal shaped antennas: a review *Encyclopedia of RF and Microwave Engineering* (Hoboken, NJ: Wiley) (https://doi.org/https://doi.org/10.1002/0471654507)

[64] Werner D H, Haupt R L and Werner P L 1999 Fractal antenna engineering: the theory and design of fractal antenna arrays *IEEE Antennas Propag. Mag.* **41** 37–58

[65] Cohen N 1997 Fractal antenna applications in wireless telecommunications *Professional Program Proc.* (Electronic Industries Forum of New England) pp 43–49

[66] Cai T, Wang G M, Zhang X F and Shi J P 2015 Low-profile compact circularly-polarized antenna based on fractal metasurface and fractal resonator *IEEE Antennas Wirel. Propag. Lett.* **14** 1072–6

[67] Pakkathillam J K and Kanagasabai M 2015 Circularly polarized broadband antenna deploying fractal slot geometry *IEEE Antennas Wirel. Propag. Lett.* **14** 1286–9

[68] Kumar Y, Gangwar R K and Kanaujia B K 2020 Characterization of CP radiations in a planar monopole antenna using tuning fork fractal slot for LTE band13/Wi-Max and Wi-Fi applications *IEEE Access* **8** 127123–33

[69] Abed T 2018 Highly compact size serpentine-shaped multiple-input–multiple-output fractal antenna with CP diversity *Antennas Propag. IET Microwaves* **12** 636–40

[70] Feng G, Chen L, Xue X and Shi X 2017 Broadband circularly polarized crossed-dipole antenna with a single asymmetrical cross-loop *IEEE Antennas Wirel. Propag. Lett.* **16** 3184–7

[71] Ta S X and Park I 2015 Crossed dipole loaded with magneto-electric dipole for wideband and wide-beam circularly polarized radiation *IEEE Antennas Wirel. Propag. Lett.* **14** 358–61

[72] Baik J, Lee T, Pyo S, Han S, Jeong J and Kim Y 2011 Broadband circularly polarized crossed dipole with parasitic loop resonators and its arrays *IEEE Trans. Antennas Propag.* **59** 80–88

[73] Feng D, Zhai H, Xi L, Yang S, Zhang K and Yang D 2017 A broadband low-profile circular-polarized antenna on an AMC reflector *IEEE Antennas Wirel. Propag. Lett.* **16** 2840–3

[74] Gou Y, Yang S, Li J and Nie Z 2014 A compact dual-polarized printed dipole antenna with high isolation for wideband base station applications *IEEE Trans. Antennas Propag.* **62** 4392–5

[75] Li R, Wu T, Pan B, Lim K, Laskar J and Tentzeris M M 2009 Equivalent-circuit analysis of a broadband printed dipole with adjusted integrated balun and an array for base station applications *IEEE Trans. Antennas Propag.* **57** 2180–4

[76] Wu Y, Liu Y and Xue Q 2011 An analytical approach for a novel coupled-line dual-band Wilkinson power divider *IEEE Trans. Microw. Theory Tech.* **59** 286–94

[77] Liu Q, Liu Y, Shen J, Li S, Yu C and Lu Y 2014 Wideband single-layer 90° phase shifter using stepped impedance open stub and coupled-line with weak coupling *IEEE Microwave Wirel. Compon. Lett.* **24** 176–8

[78] Espalin D, Muse D W, MacDonald E and Wicker R B 2014 3D printing multi-functionality: structures with electronics *Int. J. Adv. Manuf. Technol.* **72** 963–78

[79] Farooqui M F and Kishk A 2019 3D-printed tunable circularly polarized microstrip patch antenna *IEEE Antennas Wirel. Propag. Lett.* **18** 1429–32

[80] Colella R and Catarinucci L (A M Design method for wideband circularly polarized slot antennas ichel) 2020 Circularly polarized antenna in 3D printing technology to feed a wearable fully-integrated WiFi-RFID reader for biomedical applications *2020 Int. Workshop on Antenna Technology (iWAT)* (IEEE) pp 1–4

[81] Zhang Y *et al* 2019 A 3D printed circularly polarized filtering antenna *2019 IEEE Int. Symp. on Antennas and Propagation and USNC-URSI Radio Science Meeting* (IEEE) pp 1999–2000

[82] Wang K X and Wong H 2017 A wideband CP millimeter wave antenna by using 3D printed technology *2017 Int. Applied Computational Electromagnetics Society Symp. (ACES)* (IEEE) pp 1–2

[83] Jun S, Sanz-Izquierdo B, Heirons J, Mao C X, Gao S, Bird D and McClelland A 2017 Circular polarised antenna fabricated with low-cost 3D and inkjet printing equipment *Electron. Lett.* **53** 370–1

[84] Chen X, Guo Y, Qin P and Fu G 2016 22 *2016 Int. Conf. on Electromagnetics in Advanced Applications (ICEAA)* (IEEE) pp 497–500

[85] Johnson K, Zemba M, Conner B P, Walker J, Burden E, Rogers K, Cwiok K R, MacDonald E and Cortes P 2019

Digital manufacturing of pathologically-complex 3D printed antennas *IEEE Access* **7** 39378–89

[86] Sanz-Izquierdo B and Parker E A 2014 3D printing of elements in frequency selective arrays *IEEE Trans. Antennas Propag.* **62** 6060–6

[87] Jun S, Sanz-Izquierdo B and Parker E A 2016 3D printing technique for the development of non-planar electromagnetic bandgap structures for antenna applications *Electron. Lett.* **52** 175–6

[88] Nayeri P, Liang M, Sabory-Garcı R A, Tuo M, Yang F, Gehm M, Xin H and Elsherbeni A Z 2014 3D printed dielectric reflectarrays: low-cost high-gain antennas at sub-millimeter waves *IEEE Trans. Antennas Propag.* **62** 2000–8

[89] Pa P, Larimore Z, Parsons P and Mirotznik M 2015 Multi-material additive manufacturing of embedded low-profile antennas *Electron. Lett.* **51** 1561–2

[90] Kim S, Ren Y-J, Lee H, Rida A, Nikolaou S and Tentzeris M M 2012 Monopole antenna with inkjet-printed EBG array on paper substrate for wearable applications *IEEE Antennas Wirel. Propag. Lett.* **11** 663–6

[91] Tawk Y, Chahoud M, Fadous M, Costantine J and Christodoulou C G 2017 The miniaturization of a partially 3D printed quadrifilar helix antenna *IEEE Trans. Antennas Propag.* **65** 5043–51

[92] Kaddour A-S, Bories S, Bellion A and Delaveaud C 2018 3-D-printed compact wideband magnetoelectric dipoles with circular polarization *IEEE Antennas Wirel. Propag. Lett.* **17** 2026–30

[93] Farooqui M F and Shamim A Inkjet printed circularly polarized antennas for GPS applications *2014 IEEE Antennas and Propagation Society Int. Symp. (APSURSI)* pp 856–7

[94] Maimaiti M and Baktur R 2013 Inkjet printed circularly polarized patch antenna on a cylindrical surface *2013 IEEE Antennas and Propagation Society Int. Symp. (APSURSI)* (IEEE) pp 1854–5

[95] Deng S M, Wu M D and Hsu P 1995 Analysis of coplanar waveguide-fed microstrip antennas *IEEE Trans. Antennas Propag.* **43** 734–7

[96] Huang C-Y and Wong K-L 2000 Coplanar waveguide-fed circularly polarized microstrip antenna *IEEE Trans. Antennas Propag.* **48** 328–9

[97] Forma G and Laheurte J-M 1996 CPW-fed oscillating microstrip antennas *Electron. Lett.* **32** 85–86

[98] Saini R K, Dwari S and Mandal M K 2017 CPW-fed dual-band dual-sense circularly polarized monopole antenna *IEEE Antennas Wirel. Propag. Lett.* **16** 2497–500

[99] Saini R K, Bakariya P S and Kumar P 2018 Coplanar waveguide fed dual-band dual-sense circular polarized square slot antenna *Int. J. RF Microwave Comput.-Aided Eng.* **28** e21503

[100] Sze J-Y, Wong K-L and Huang C-C 2003 Coplanar waveguide-fed square slot antenna for broadband circularly polarized radiation *IEEE Trans. Antennas Propag.* **51** 2141–4

[101] Sze J Y and Pan S P 2011 Design of CPW-fed circularly polarized slot antenna with a miniature configuration *IEEE Antennas Wirel. Propag. Lett.* **10** 1465–8

[102] Hussaini A S *et al* 2015 Green flexible RF for 5G *Fundamentals of 5G Mobile Networks* 1st edn, Ed J Rodriguez (New York: Wiley) pp 241–72

[103] Statement: Improving Consumer Access to Mobile Services at 3.6 GHz to 3.8 GHz (available at: www.ofcom.org.uk/consultations-and-statements/category-1/future-use-at-3.6-3.8-ghz) (Accessed 5 July 2021)